JOURNAL OF CATALYSIS 123, 206–214 (1990)

# The Mechanism of Methane Formation from the Reaction between Graphite and Hydrogen

Z. J. PAN AND R. T. YANG[1]

*Department of Chemical Engineering, State University of New York at Buffalo, Buffalo, New York 14260*

Received September 6, 1989; revised November 28, 1989

Monolayer etch pits formed on the basal plane of graphite by hydrogen are hexagonal in shape and are bounded by $\{10\bar{1}l\}$ zigzag edge faces. The reaction is also studied by using extended Hückel molecular orbital (EHMO) calculations with geometry optimization, where H atoms are added to the edge surface carbon and these carbon atoms are allowed to deform from the original positions corresponding to the graphite structure to reach the equilibrium positions. The EHMO/geometry optimization results indicate that the zigzag edge face is more reactive than the $\{11\bar{2}l\}$ armchair face before and after one H is chemisorbed on the surface atom. However, a reversal in the relative reactivity occurs after the second H addition; the C–C bond on the armchair face becomes weaker and carbon atoms become more reactive for the third H chemisorption. Breakage of C–C bonds takes place upon the third H addition, and this step is the rate-limiting step for $CH_4$ formation.


## INTRODUCTION

Among the important gas–carbon reactions, the C–$H_2$ reaction is the least understood (*1*). The predominant reaction product is $CH_4$ at temperatures below 1800 K. In addition to possible industrial applications for this reaction, an understanding of this reaction would also help our understanding of the catalyzed methanation reaction where the hydrogenation of surface carbon is the rate-limiting step (*2*). A number of studies have been reported on the "uncatalyzed" C–$H_2$ reaction (*1, 3–6*); however, evidence has been shown that the reaction was caused by impurities at concentrations as low as parts per million levels (*6*), and widely different activation energies ranging from 22 (*6*) to 85 kcal/mol (*4*) have been reported. Nevertheless, three possible mechanisms for the uncatalyzed reaction have been postulated (*3–7*), all requiring successive, dissociative chemisorption of $H_2$ on the prismatic edge faces of graphite.

A number of experimental studies have also been reported on the chemisorption of hydrogen on graphite at temperatures up to 1495°C ((*8–11*); and references cited in (*9*)). The experimental results indicate that hydrogen dissociatively chemisorbs on the edge planes of graphite, not on the basal plane. The results of Bansal *et al.* (*9*) showed that the chemisorption occurs in four stages, each with a distinct activation energy (from 5.7 kcal/mol increasing to 30.4 kcal/mol) indicating different edge sites and/or one vs two hydrogen atoms on each site. Theoretical studies of chemisorption of hydrogen on graphite has been performed using various approximate molecular orbital (MO) calculations (*12–17*) with the conclusion that only edge planes can chemisorb hydrogen (*17*). In the study by Chen and Yang (*17*), only one H atom was chemisorbed on the edge carbon atom and the surfaces of the edge planes were rigidly held in positions corresponding to the bulk graphite structure. This was relaxed in this study where the surface carbon atoms were allowed to equilibrate at the positions corresponding to the minimum potential energy.

[1] To whom all correspondence should be addressed.



0021-9517/90 $3.00

### EHMO/GEOMETRY OPTIMIZATION

The extended Hückel molecular orbital (EHMO) theory was used to follow the bonding changes for the graphite–hydrogen system. The calculations were based on a program originally written by Hoffmann, and the version modified by Howell *et al.* (*18*) was used. The computations were performed on a VAX 8700 computer.

The principles and applications of EHMO to chemisorption and catalysis have been described in several reviews (*19, 20*). Due to its simplicity, the EHMO has been used to provide valuable semiquantitative information for complex systems on catalysis (*21, 22*) and metal clusters (*23, 24*).

EHMO is a semiempirical MO scheme in which the diagonal elements of the Hamiltonian matrix ($H_{ii}$) in the Slater orbital are taken as the valence state ionization energy (VSIE) (or the negative ionization potential). The off-diagonal elements are taken to be proportional to the average of the two relevant atomic ionization potentials ($H_{ii}$ $H_{jj}$) and the overlap integral ($S_{ij}$), i.e.,

$$H_{ij} = \tfrac{1}{2}KS_{ij}(H_{ii} + H_{jj}),$$

where $K$ is an empirical constant usually taken as 1.75. In this work, the binding energy between graphite and atomic hydrogen was calculated as the difference between the total energy of the bonded atoms (adatoms plus graphite) and that of the isolated graphite and hydrogen, i.e., $E_{C\text{–}H} = E_{total} - E_C - E_H$. The overlap populations between two atoms were calculated by the Mulliken procedure (*25*). All calculations were performed by means of charge iteration according to

$$H_{ii} = H_{ii}^0 + (\text{sense}) \times (\text{charge}),$$

where $H_{ii}$ is the diagonal element of the Hamiltonian matrix in the Slater orbital, $H_{ii}^0$ is the value of $H_{ii}$ from the previous iteration cycle, "sense" is a constant taken to be 0.1, and "charge" is the total charge of atom $i$ which is zero in the first cycle for all atoms. The orbital exponents were 1.625 for both $2s$ and $2p$ orbitals of carbon, and 1.3 for the $1s$ orbital of hydrogen.

For geometry optimization, the EHMO program (*18*) was modified to be incorporated as a subroutine into the optimization program "BCONF" which is available from IMSL (*26*). The BCONF program employs the quasi-Newton method to search for the minimum value of a function of $N$ variables subject to given bounds for the variables. In the models of one to two H chemisorbed on the edges of graphite, two to four variables (bond lengths and bond angles as described below) needed to be optimized for the minimum energy. These variables were subject to the constraints that no overlapping of atoms was allowed. Depending on the chemisorption model, 30 to 60 times of function calculation were needed to reach the minimum, requiring 1 to 2 hr of CPU time on a VAX 8700 computer.

#### *Graphite/Hydrogen Models*

The three graphite models employed in the EHMO calculations are shown in Fig. 1. Model A contains 24 C atoms and was used for hydrogen chemisorption on the $\{11\bar{2}l\}$ (armchair) edge plane. Model B contains 25 C atoms and was used for hydrogen chemisorption on the $\{10\bar{1}l\}$ (zigzag) edge plane. Model C contains 36 C atoms and was used only for the purpose of examining the end and edge (with and without hydrogen saturation) effects.

EHMO/geometry optimization calculations were performed on the three graphite models and on these models with one and two H atoms attached to the edge carbon atom. With H attached, the edge carbon atom was allowed to deform from its original position (as in the graphite structure) in order to reach the most stable position corresponding to the energy minimum. The number of variables in geometry optimization was reduced by considering the symmetry constraint, i.e., the symmetry between the C–H bond(s) and the adjoining C–C bonds. The number of variables varied

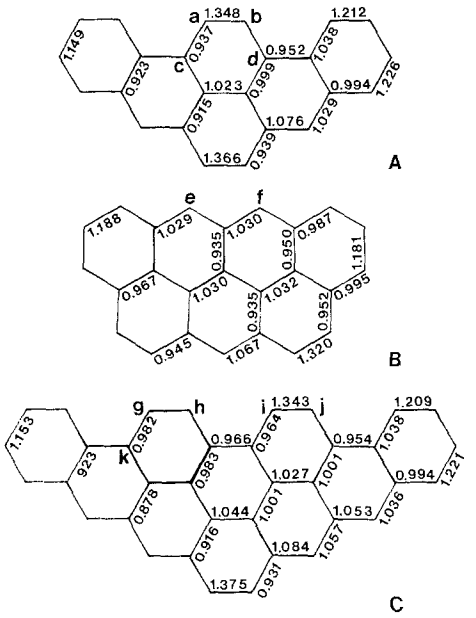


FIG. 1. Graphite models with C–C bond overlap populations from EHMO calculations; all results are symmetrical between left and right.

from two to four depending on the graphite/hydrogen model. For one H on the zigzag edge carbon, there are two variables: C–H bond length and C–C bond length. The number increased to three for two H atoms on the zigzag edge carbon: C–H bond length, H–C–H bond angle, and C–C bond length. The number of variables was higher for the armchair edge. Three variables were needed for optimizing one H on each armchair edge carbon: C–H bond length and the lengths of the two adjoining C–C bonds, and four variables were needed for two H on each armchair edge carbon: C–H bond length, H–C–H bond angle, and the lengths of the adjoining C–C bonds.

## EXPERIMENTAL AND RESULTS

The carbon used in this study was a natural single-crystal graphite from Ticonderoga, New York. This graphite was employed due to its well-defined crystalline structure and its ability to be cleaved into specimens thin enough for transmission electron microscope (TEM) observation while maintaining a large single-crystal basal plane area. The techniques used to prepare the samples for TEM observation have been discussed in detail elsewhere (*27*).

Monolayer (3.35 Å depth) etch pits were formed by the attack of hydrogen on the basal plane surface of graphite. These etch pits originated from lattice vacancies in the basal plane. The etch pits were made visible by decorating gold nuclei on the edges of the pits followed by TEM observation. The details of the technique were also discussed elsewhere (*27*).

The hydrogen etch reaction was carried out in a silicon carbide furnace, in which the graphite sample was supported on a sapphire plate. Because of the high temperature required for the reaction (above 1400°C), extremely stringent measures were taken to remove the traces of impurity gases in hydrogen and helium carrier ($O_2$, $H_2O$, $CO_2$, and CO) and to avoid the dust particles originating from the reactor walls. Ultrahigh purities of hydrogen (99.999% minimum) and helium (99.999% minimum) were used. The hydrogen was further treated in a Pd catalyst bed to remove impurity $O_2$. The He and treated $H_2$ were then separately passed through a long-residence-time liquid-$N_2$ trap which contained three separate beds of activated carbon, 13X zeolite, and 5A zeolite. The reactor was a "high-purity" alumina tube (McDaniel 998 alumina), which was further lined with graphoil (a high-purity graphite foil). With these treatments, control experiments using helium alone showed no etch pits at the reaction temperature of 1435°C.

Using the purification system above, no etch pits were formed on the basal plane of graphite by 1 atm $H_2$ at 1435°C for prolonged periods of time (up to 14 hr). In order to facilitate etch pit formation, a tungsten foil was placed adjacent to (but not in contact with) the graphite sample. The presence of tungsten helped the dissociation of $H_2$ so an equilibrium amount of H atoms could be approached (the equilibrium

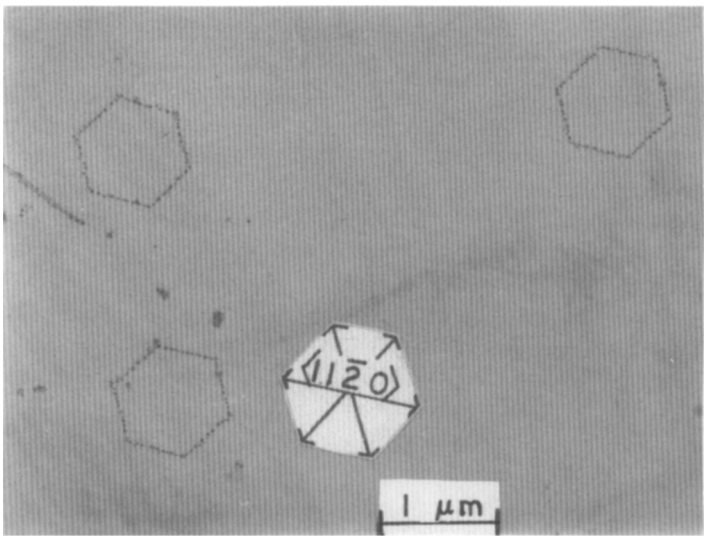


FIG. 2. TEM picture of gold-decorated etch pits on the basal plane of graphite formed by reaction with hydrogen at 1435°C for 2 hr. The zigzag plane directions were determined by electron diffraction.

partial pressure of H at 1800 K and 1 atm is $3.56 \times 10^{-4}$ atm).

A typical TEM picture of gold-decorated etch pits on the basal plane of graphite formed by 1 atm $H_2$ at 1435°C (2 hr) is shown in Fig. 2. These pits were formed by H atoms. By matching the TEM picture with the selected-area electron diffraction pattern of the graphite, the orientation of the etch pits could be determined. The electron diffraction result is also shown in Fig. 2, where the $\{10\bar{1}l\}$ (zigzag) directions are labeled. This result showed that all hexagonal etch pits were bounded by zigzag edges. This result was possible only if the armchair edges were preferentially attacked by H atoms to form methane.

## EHMO RESULTS AND DISCUSSION

The EHMO results to be shown here are based on graphite models A and B (Fig. 1), where H is chemisorbed only on the armchair sites *a*, *b* (model A) and zigzag sites *e*, *f* (model B). First, it must be shown that these H/graphite models are adequate to represent the chemisorption of H on large armchair and zigzag planes of graphite. (A single layer of graphite is adequate to represent the multilayer graphite due to the large interlayer separation, 3.35 Å.) The effects of ends and edges are to be addressed, i.e., the effects of the size of the graphite model and whether the other edge carbon atoms are also bonded to hydrogen.

The effect of the size of the graphite model has been studied earlier by Bennett *et al.* (*28*) using EHMO and CNDO methods, and it was shown that 18 carbon atoms were adequate to represent the basal plane of graphite. The overlap populations (which reflect the covalent bond strengths) between models A and C may be compared to see the effects of the size of graphite on the edge carbon (Fig. 1). It is seen that the armchair surface bonds are virtually the same in these two models, e.g., 1.348 for bond *a*–*b* (in model A) and 1.343 for bond *g*–*h* or *i*–*j* (in model C). Thus, carbon atoms *a* and *b* in model A are adequate to represent the armchair face of graphite. In studying the chemisorption on the basal plane, the edge effects were minimized by saturating with H (*15, 16*); Illas *et al.* (*15*) and Barone *et al.* (*16*) used naphthalene ($C_{10}H_{10}$), pyrene ($C_{16}H_{16}$), and coronene ($C_{24}H_{24}$) as the models for graphite. Our EHMO/geometry

TABLE 1

Results on Bond Length (in Å) from EHMO/ Geometry Optimization for One H Chemisorbed on Each Edge Carbon in Different Graphite Models

| | 1[a] | 2[a] | 3[a] |
|---|---|---|---|
| C–H bond | 0.7552 | 0.7538 | 0.7546 |
| C–C bond (a–c or k–g) | 1.606 | 1.623 | 1.625 |
| C–C bond (a–b or g–h) | 1.371 | 1.357 | 1.364 |

[a] With reference to Fig. 1, case 1 is for H on armchair sites *a* and *b* in model A; case 2 is for H on armchair sites *g, h, i,* and *j* in model C; case 3 is for H on armchair sites *a* and *b* in model A where all edge carbon atoms except *a* and *b* are saturated with one trigonal C–H bond at 0.8 Å.

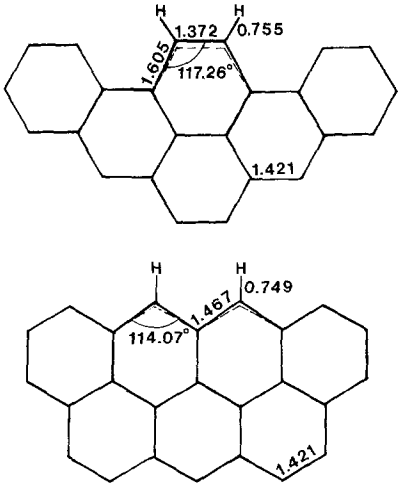


FIG. 3. EHMO/geometry optimization results showing the equilibrium bond lengths (in Å) and bond angles with one H chemisorbed on the two edge planes.

optimization results on the edge effects are summarized in Table 1. One H is chemisorbed on each of the armchair sites *a*, *b* (in model A), *g, h, i, j* (in model C), and only these atoms are allowed for geometry optimization. Case 3 in Table 1 is for all edge atoms in model A except *a* and *b* to be presaturated with one H. The results shown in Table 1 indicate that sites *a* and *b* in graphite model A are adequate for studying hydrogen chemisorption on the armchair plane of graphite, with minimal effects of chemisorbed hydrogen on other sites. A similar conclusion can be reached for the zigzag (*e* and *f*) sites in graphite model B. Thus, all EHMO/geometry optimization calculations are performed on sites *a*, *b* in model A and sites *e*, *f* in model B.

The EHMO/geometry optimization results for one H and two H chemisorbed on each of the edge carbon atoms are shown respectively in Figs. 3 and 4. The deformation of the edge surfaces (from the graphite structure) is small with one H chemisorbed on each edge atom (Fig. 3), but becomes large after the addition of the second H (Fig. 4). On both edge planes, the C–C bonds are lengthened (or weakened) upon H chemisorption, being more so with two H.

The strength of a covalent bond is measured by the overlap population. The overlap population results from the geometry optimization calculations are summarized in Fig. 5, where only edge surface bonds are shown. (All other C–C bonds remain nearly the same as those given in Fig. 1, i.e., they are unperturbed.)

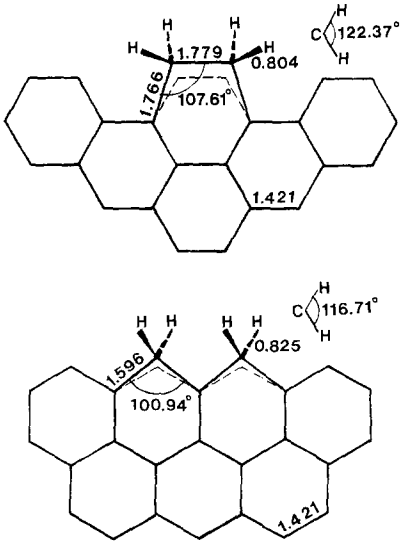


FIG. 4. EHMO/geometry optimization results showing the equilibrium bond lengths (in Å) and bond angles with two H chemisorbed.

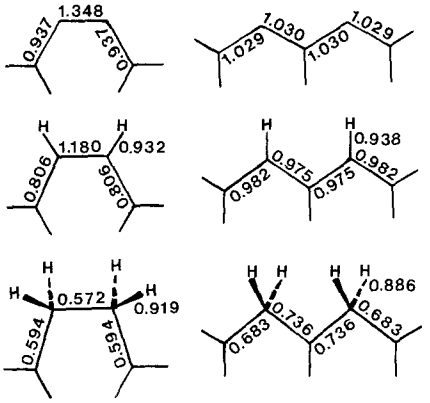


FIG. 5. EHMO/geometry optimization results for bond overlap population on the armchair and zigzag faces of graphite with zero, one, and two H chemisorbed.

The total overlap population (TOP) around a carbon atom is an indicator of its ability (or lack of ability) to form a new covalent bond, and hence is an indicator of its activity. The difference between the TOP value from the maximum possible value has the same meaning as the free valence index, which is the reactivity index for reaction with free radicals. The TOP values are shown in Table 2 for no H, one H and two H bonded to each edge carbon. On a clean surface, the TOP on the zigzag edge atom is lower than that of the armchair atom, hence the zigzag face is more reactive or more capable of chemisorbing hydrogen. After one H addition, the same comparison holds but with a smaller difference. After two H addition, the situation is reversed and the armchair edge atom becomes more reactive because of its lower TOP. Moreover, the TOP results in Table 2 indicate that the second H addition is considerably more difficult than the first H addition, since the TOP values on both armchair and zigzag faces increase substantially after the first H addition. This result is consistent with the experimental observation that it is likely each edge site chemisorbs only one hydrogen atom (*10*).

TABLE 2

Total Overlap Population (TOP) Around the Edge Carbon Atom and C–H Bond Energy on Different Graphite Faces from EHMO/Geometry Optimization

| | $\{11\bar{2}l\}$ armchair | $\{10\bar{1}l\}$ zigzag |
|---|---|---|
| TOP without H | 2.321 | 2.059 |
| TOP, one H chemisorbed | 2.918 | 2.856 |
| TOP, two H chemisorbed | 3.004 | 3.191 |
| C–H bond, kcal/mol (one H added) | 84.82 | 89.98 |
| C–H bond, kcal/mol (two H added) | 74.85 | 60.33 |

The overlap populations of all C–C bonds in the graphite are nearly unity except that connecting two armchair edge atoms (Fig. 1 or Fig. 5). These armchair surface bonds have a value of 1.34, which is close to the value of a double bond. (The OP in the ethylene double bond is 1.299, Ref. (*18*)). This indicates that in addition to the $sp^2$–$sp^2$ $\sigma$ bond (that exists in bulk graphite), some overlap between the two neighboring free $sp^2$ electrons or a $\pi$ bond formed by localization of the two $2p_z$ orbitals may have occurred.

The C–H bond energies (calculated as the minimum potential energies from graphite and the H atom) are also given in Table 2. These bond energies are consistent with the C–H bond overlap populations given in Fig. 5.

With reference to Fig. 5, it is seen that the C–C bonds on the edge surfaces are progressively weakened as H atoms are added. The first chemisorbed H forms a $sp^2$–$s$ $\sigma$ bond, whereas upon the second H addition, the C–H bonds are formed by $sp^3$–$s$ $\sigma$ bonds, which are weaker than the $sp^2$–$s$ bonds. It is significant to compare the surface C–C bonds between the armchair and zigzag faces after two H are added. The C–C bond on the armchair face is now formed by $sp^3$–$sp^3$ overlap $\sigma$ bond, whereas the zigzag face is formed by $sp^3$–$sp^2$ bonds. The $sp^3$–$sp^3$ bonds (as in diamond structure) are weaker and longer (1.54 Å) compared to the $sp^2$–$sp^2$ bonds (as in graphite, 1.42 Å). This comparison is consistent with our results on two H chemisorption shown on Fig. 4. Here the C–C bond length on the armchair face is 1.779 Å (a $sp^3$–$sp^3$ bond)

compared with that on the zigzag face of 1.596 Å (a $sp^3$–$sp^2$ bond).

## MECHANISM FOR METHANE FORMATION

The mechanism for $CH_4$ formation by successive hydrogen chemisorption is shown in Fig. 6 for the two edge planes of graphite. In both cases, the surface C–C bond cleavage is required for the third H addition, after which dangling bonds remain and $CH_4$ formation is energetically very favorable. Judging from the total overlap population (Table 2), the edge surface carbon atoms become saturated (hence the free valence reaches a minimum) and inactive for further chemisorption after two H addition. Consequently, the third H addition or the C–C bond breakage step is the rate-limiting step for methane formation.

Although the EHMO method is semiquantitative where the results depend on the parameters used for the calculation, comparisons based on the results using the same parameters are considered reliable. The EHMO results on the H/graphite system (Table 2 and Fig. 5) show that the first H addition is relatively easier than the second H addition on both edge faces of graphite. The zigzag edge atoms are more reactive for hydrogen chemisorption for both first and second H addition. However, a most significant result from this calculation is that there is a reversal in the relative reactivity between the two edge planes upon the second H addition. The overlap population of the C–C bond on the armchair face is the strongest before and after the first H addition, decreasing from 1.348 to 1.180, compared to 1.03 (no H) and below 1 (one H added) for the zigzag face and nearly 1 for all bulk C–C bonds. After the second H addition, the C–C overlap population of the armchair face is decreased to 0.572, which is the lowest among all C–C bonds (shown in Fig. 5). The cleavage of this C–C bond is hence the easiest. The corresponding values for the zigzag face are 0.683 and 0.736 (Fig. 5); hence the C–C bonds are more difficult to cleave. These theoretical results are consistent with the experimental observation that hexagonal etch pits are formed, which are bounded by zigzag edges of graphite. Conversely, this experimental result indicates that the third H addition which requires C–C bond breakage is the rate-limiting step in methane formation.

The formation of the two $CH_3$ groups on the armchair face (Fig. 6) might appear to be sterically unfavorable due to possible H–H interactions from the neighboring $CH_3$ groups. However, our EHMO (without geometry optimization) results showed that the formation of such a structure is entirely feasible with no H–H interactions. For example, with the C–C bond length of 1.55 Å and the C–H bond length of 0.805 Å in the two $CH_3$ groups, both located symmetrically 15° from the upright position (with the two C–C bonds bending toward each other), the energy is lowered by 27.2 eV by the addition of two H atoms (adding H on the two $CH_2$ to form two $CH_3$ groups in Fig.

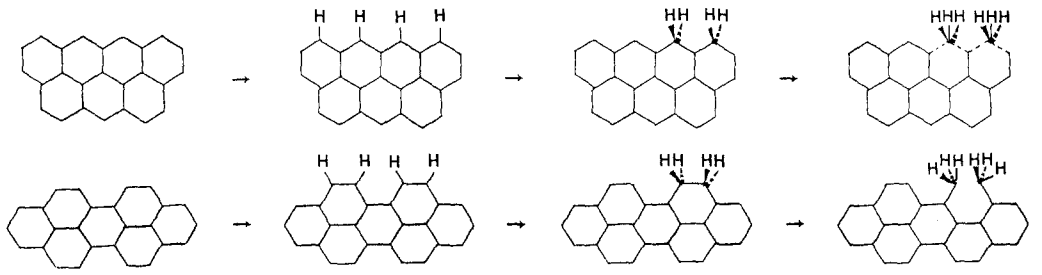


FIG. 6. Mechanism for methane formation on zigzag (upper) and armchair (lower) faces by successive H addition. C–C bond breakage occurs upon the third H addition.

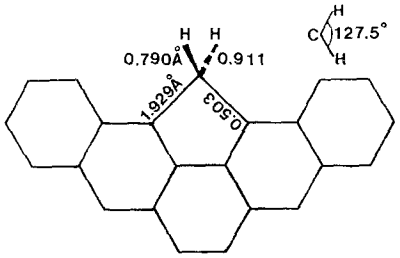


FIG. 7. EHMO/geometry optimization results for $C_5$ ring formed on the armchair face resulting from cleavage of the C–C bond upon a third H addition followed by cyclization. Bond lengths and overlap populations are shown.

6), and the nearest H–H distance in this structure is 1.6 Å with no overlap population. Nonetheless, an alternative pathway may be possible which does not involve the simultaneous formation of two $CH_3$ groups (as suggested by an anonymous reviewer). Since the C–C bond on the armchair face is the weakest one, as we have shown, this bond may be broken by the addition of only one H atom, forming a $CH_3$ and a $CH_2$. The $CH_3$ is rapidly detached to form $CH_4$ (as in the pathway suggested above) while the $CH_2$ undergoes cyclization to form a $C_5$ ring on the armchair face, shown in Fig. 7. Figure 7 shows the results of EHMO/geometry optimization. The C–C bond overlap population is further lowered to 0.503 and hence is more favorable to cleavage compared to the zigzag face.

The successive H addition may originate from H atoms or by dissociative chemisorption of $H_2$; the EHMO results from this study should be equally applicable to both cases. For graphitic carbon in contact with metals, the spillover H may be the source for H (*29*), and the EHMO results remain applicable. It has been shown, however, that H spillover does not occur on the basal plane of graphite (*30*) and could only occur on the prismatic faces of graphite (*29*).

ACKNOWLEDGMENTS

This work was supported by the National Science Foundation under CBT-8703677. We thank Mr. J. P. Chen for helpful discussions.

REFERENCES

1. Walker, P. L., Jr., Rusinko, F., and Austin, L. G., *in* "Advances in Catalysis" (W. G. Frankenburg, V. I. Komarewsky, and E. K. Rideal, Eds.), Vol. 2, p. 133. Academic Press, San Diego, 1959.
2. Bell, A. T., *in* "Proceedings, 9th International Congress on Catalysis" (M. J. Phillips and M. Ternan, Eds.), Vol. 5, p. 134. Chem. Institute of Canada, Ottawa, 1988.
3. Zielke, C. W., and Gorin, E., *Ind. Eng. Chem.* **47,** 820 (1955).
4. Hedden, K., *Z. Elektrochem.* **66,** 652 (1962).
5. Breisacher, P., and Marx, P. C., *J. Amer. Chem. Soc.* **85,** 3518 (1963).
6. Imai, H., Nomura, S., and Sasaki, Y., *Carbon* **13,** 333 (1975).
7. Tomita, A., and Tamai, Y., *J. Phys. Chem.* **78,** 2254 (1974).
8. Walker, P. L., Jr., Bansal, R. C., and Vastola, F. J., *in* "The Structure and Chemistry of Solid Surfaces," p. 81. Wiley, New York, 1969.
9. Bansal, R. C., Vastola, F. J., and Walker, P. L., Jr., *Carbon* **9,** 185 (1971).
10. Biederman, D. L., Miles, A. J., Vastola, F. J., and Walker, P. L., Jr., *Carbon* **14,** 351 (1976).
11. Sen, A., and Bercaw, J. E., *J. Phys. Chem.* **84,** 465 (1980).
12. Messmer, R. P., and Bennett, A. J., *Phys. Rev. B* **6**(2), 633 (1972).
13. Dovesi, R., Pisani, C., Ricca, F., and Roetti, C., *J. Chem. Phys.* **65,** 3075 (1976).
14. Dovesi, R., Pisani, C., and Roetti, C., *Chem. Phys. Lett.* **81,** 498 (1981).
15. Illas, F., Sanz, F., and Virgili, J., *J. Mol. Struct.* **94,** 79 (1983).
16. Barone, V., Lelj, F., Minichino, C., Russo, N., and Toscano, M., *Surf. Sci.* **189/190,** 185 (1987).
17. Chen, J. P., and Yang, R. T., *Surf. Sci.* **216,** 481 (1989).
18. Howell, J., Rossi, A., Wallace, D., Haraki, K., and Hoffmann, R., Forticon 8, QCPE No. 517, Quantum Chemistry Program Exchange, Indiana University, Dept. of Chemistry, 1988.
19. Baetzold, R. C., *J. Catal.* **29,** 129 (1973).
20. Baetzold, R. C., *in* "Advances in Catalysis" (D. D. Eley, H. Pines, P. B. Weisz, Eds.), Vol. 25, p. 1. Academic Press, New York, 1976.
21. Kusuma, T. S., and Companion, A. L., *Surf. Sci.* **195,** 59 (1988).
22. Casalone, G., Merati, F., and Tantardini, G. F., *Chem. Phys. Lett.* **137,** 234 (1987).
23. Mitchell, G. F., and Welch, A. J., *J. Chem. Soc. Dalton Trans.* **5,** 1017 (1987).
24. King, R. B., *J. Comput. Chem.* **8,** 341 (1987).
25. Mulliken, R. S., *J. Chem. Phys.* **23,** 1833 (1955).
26. FORTRAN Subroutines for Mathematical Applications, IMSL Problem-Solving Software, Inter-

national Mathematical and Statistical Libraries, Version 1.0, April 1987.
27. Yang, R. T., *in* "Chemistry and Physics of Carbon" (P. A. Thrower, Ed.), Vol. 19, p. 163. Dekker, New York, 1984.
28. Bennett, A. J., McCarroll, B., and Messmer, R. P., *Surf. Sci.* **24,** 191 (1971); *Phys. Rev. B.* **3,** 1397 (1971).
29. Robell, A. J., Ballou, E. V., and Boudart, M., *J. Phys. Chem.* **68,** 2748 (1964).
30. Goethel, P. J., and Yang, R. T., *J. Catal.* **101,** 342 (1986).